Delft University of Technology

Rider control identification in cycling taking into account steering torque feedback and sensory delays

Dialynas, Georgios; Christoforidis, Christos; Happee, Riender; Schwab, A. L.

Rider control identification in cycling taking into account steering torque feedback and sensory delays

Georgios Dialynas, Christos Christoforidis, Riender Happee & A.L. Schwab

Published online: 11 Mar 2022.

Submit your article to this journal

Article views: 976

View related articles

View Crossmark data

IAVSD

Taylor & Francis
Taylor & Francis Group

Rider control identification in cycling taking into account steering torque feedback and sensory delays

Georgios Dialynas [iD][a], Christos Christoforidis[a], Riender Happee [iD][b] and A.L. Schwab [iD][a]

[a]Biomechanical Engineering, Delft University of Technology, Delft, The Netherlands; [b]Cognitive Robotics, Delft University of Technology, Delft, The Netherlands

ABSTRACT

Experiments and human rider models were used to investigate bicycle balance and steering using visuo/vestibular motion and proprioceptive feedback taking into account sensory delays. An instrumented steer-by-wire bicycle designed and built at the TU Delft bicycle laboratory was used to investigate rider responses with and with reduced steering torque feedback. Steering responses and bicycle motions were measured perturbing balance with impulsive forces at the seat post. The rider was commanded to follow a straight lane at unstable (2.6 and 3.7 ms^{-1}) and stable speeds (4.5 and 5.6 ms^{-1}). Bicycle speed was controlled with an electric drive and cruise control. Balance and steering responses could well be captured by linear impulse response functions which were consistent across participants. The impulse response functions were used to develop neuromuscular control models capturing rider–bicycle interaction. The Carvallo–Whipple bicycle model was extended with rider inertia and an additional degree of freedom for the steer-by-wire system. Rider behaviour was modelled as a balance and heading controller. This controller used visuo/vestibular motion feedback of roll angle and roll rate, heading angle and heading rate, and proprioceptive feedback of steering angle, velocity and torque. Results showed that the rider model followed the necessary stability condition of steer into the fall and was capable of stabilising the bicycle. Sensory delays had a negative effect on the model fit, which was resolved with an internal model and prediction algorithm. A model without steer angle and steer velocity feedback could not well capture the human response at the highest speeds and the absence of torque feedback had similar effects for all speeds, supporting the relevance of steer angle and torque feedback in bicycle control.

1. Introduction

The balance and control of bicycles in motion is a skill that the majority of the population acquires since early childhood. However the way humans control and balance bicycles is only partially understood [1,2]. From the first appearance of the modern bicycle in the late 1880s until now, dynamic models of uncontrolled bicycles have provided fundamental

CONTACT Georgios Dialynas ✉ georgedialynas@hotmail.gr

insights into bicycle stability in relation to speed and geometry [3,4]. However, additional knowledge on human control is required to design safer bicycles and to assess new safety systems (e.g. steer assist functionalities). The latter can greatly improve bicycle safety and reduce single-bicycle accidents [5] particularly important for elderly cyclists [6].

Research in the field of cybernetics started in the 1950s to advance aircraft technology and understand pilot control. McRuer and Krendel [7] were amongst the first to model the human operator as a servo system with time delay. The so called 'McRuer cross over model' was later extended to the 'McRuer precision model' capturing neuromuscular dynamics and delays [8]. Results showed that for a range of controlled system dynamics, humans were able to realise a closed loop response resembling a first-order system. Among the first researchers who focused on the manual control of bicycles were Van Lunteren et al. [9]. They used a stationary bicycle simulator and system identification techniques to identify the parameters of a proportional-integral-derivative (PID) rider controller with delay. However, their bicycle simulator had no visual display and the rider model has not been experimentally validated. Weir [10] developed a cross-over model for Sharp's [11] motorcycle model. He concluded that a simple linear steer torque controller that takes into account the lean angle is sufficient for balancing a motorcycle in motion. Eaton [12] later conducted experiments to validate these models [10,11]. Despite the fact that he excluded the lean torque and used only the lean angle stabilisation loop results were promising. Control parameters could be estimated with low uncertainty and steer torque responses were fitted well. Jason Moore [13] studied rider control during simple bicycle maneuvers. He constructed an instrumented bicycle measuring the applied steer torque and conducted a series of lateral perturbation experiments on a treadmill and on a pavilion floor. This extensive dataset was used to identify both the plant and the rider model. Some of the methods and modelling approaches that he utilised in his thesis were also adopted herein. Hess et al. [14] introduced task independent handling quality metrics for bicycle control. Using these metrics, they developed a rider model with five gains, two second-order filters, and a preview time. Soudbakhsh et al. [15] mounted a stationary bicycle on a motion platform and applied lateral sweep perturbations to capture the rider's responses. Their conclusion was that it is impossible to stabilise the stationary bicycle only with upper body movements, whereas with additional steering control riders can balance the bicycle. Chu et al. [16] measured the steering and roll angle of a bicycle and used a model predictive controller as a rider model applying steering and leaning torques. Wang et al. [17] conducted experiments in order to analyse the stability and control of a rider–bicycle system and developed a rider model controlling body lean torque. Building upon [13] Schwab et al. [18] modelled the bicycle rider using lateral force perturbation experiments to explore the potential feedback of sensory cues during the bicycle balancing task. Even though the rider control model seemed to mimic human control in a natural way, there were limitations in this study: The first limitation was that experiments were conducted on a narrow treadmill and, as reported, this may have created bias in the control behaviour. The second limitation was that sensory delays (e.g. visual, vestibular and proprioceptive) were omitted. A third limitation was that steering torque feedback was not considered.

In the present study, we build upon the work by Schwab et al. [18] including delays in the sensory paths and exploring the role of steering torque feedback. We performed new experiments on a wide bicycle lane instead of a treadmill, using the experimental steer-by-wire bicycle developed by Dialynas et al. [19]. We reconfigure the parameters of the

Carvallo–Whipple bicycle model [3] to the physical properties of the steer-by-bicycle. We use the gathered data to develop a novel rider control model, which is not only able to take into account sensory delays but also to adapt to different steering dynamics to evaluate the role of steering torque feedback in rider control.

This study has three main objectives; the first is to design a rider control model which takes into account steer torque feedback and sensory delays. We include a *predictor model*, as frequently employed in human motor control studies to compensate sensory delays, and to estimate the current system state [20–23]. The second is to examine the ability of humans to adapt to altered steering dynamics even when feedback is intermittent and delayed. The third is to evaluate the effect of handlebar torque and position feedback. The paper is organised as follows: First, the experimental set-up and experimental procedure are presented. Next, the methods and results are presented. The article ends with a discussion and conclusion highlighting the main findings. A preliminary analysis of this research was published as an MSc thesis [24]. All data presented herein have been reanalysed and results were extended.

2. Methods

2.1. Description of the experimental set-up

At TU Delft we designed and built a steer-by-wire bicycle [19] equipped with multiple sensors measuring most bicycle states and rider control inputs required for rider model identification (see Figure 1(a)). A pulling rope mechanism with a force transducer in series was used to manually apply lateral impulsive forces at the seat post (see Figure 1(b)). The bicycle is equipped with rear wheel hub motor and a cruise control system, so the subjects did not need to pedal to maintain a constant speed. Measurements of the inertial measurement unit (IMU), steering angle encoder, torque sensor and rope force transducer were logged at 1000 Hz. Steering angle δ was directly measured from the absolute encoder of the upper front assembly, while the roll angle ϕ was estimated from the measured roll rate $\dot{\phi}$ as described by Sanjurjo et al. [25].

2.2. Description of the steer-by-wire controller

The steer-by-wire system enables flexible adjustment of steering actions and haptic feedback (steering torque). In this paper we mimic normal steering motion, where the fork rotation is approximately equal to the handlebar rotation. We manipulate steering torque, where the controller was programmed to approximate: 1) normal steering torque (haptics on) and 2) reduced steering torque (haptics off) isolating the rider from torques resulting from tyre to road interaction. The applied controller is described by Dialynas et al. [19] and here we adopted the parameters ($K_{PH} = 0.9, K_{PF} = 2, K_{DH} = 0.012, K_{DF} = 0.025$ Nms/rad in normal steering with K_{PH} and $K_{DH} = 0$) in the haptics off condition.

2.3. Experimental procedure

Eighteen males and two females (age $= 26 \pm 2$ years) volunteered in this study. To assure safety, all participants were requested to wear protective equipment, which includes a
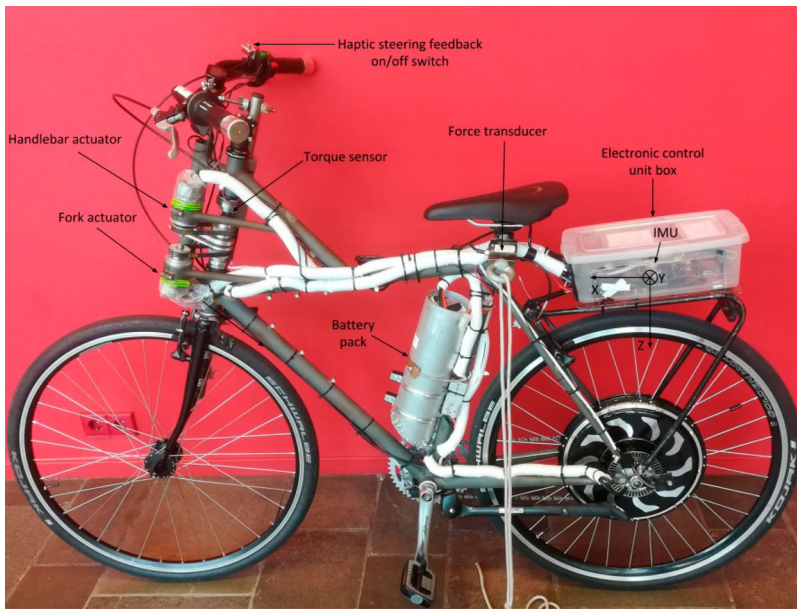
(a)

(b)

Figure 1. Steer-by-wire bicycle (top) and experimental conditions (bottom) where the experiment coordinator (bottom) cycling next to the steer-by-wire bicycle applies an impulsive lateral force with a rope.

standards-approved bike helmet, knee and elbow pads. All subjects gave informed consent according to the guidelines of the TU Delft human research ethics committee. They reported that they did not experience any kind of pain or injury in the year before the experiments. The mean weight of the participants (82.1 ± 6.4 kg) was close to the European
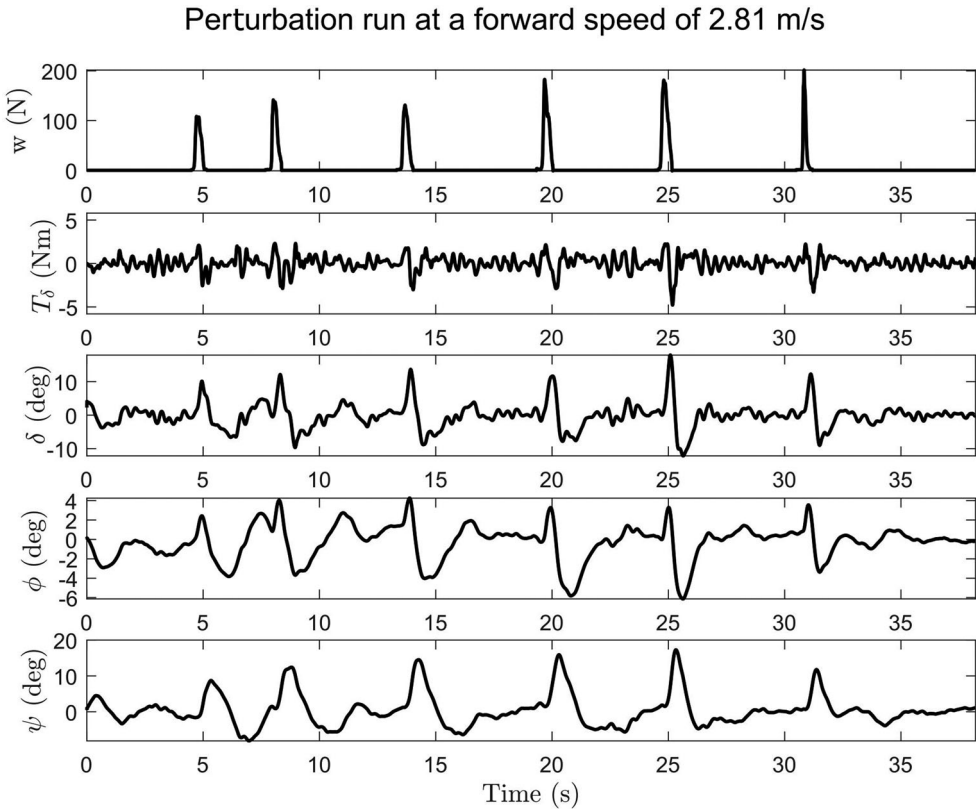
Figure 2. Example measurements of the lateral disturbance force w, rider applied steer torque T_δ, steer angle δ, roll angle ϕ and heading ψ at a forward velocity of 2.81 ms^{-1} (first 40 seconds).

population [26], whereas the height (181 ± 7 cm) was close to the mean height of young European men [27].

Each experimental trial consisted of four different speeds (i.e. 2.6, 3.7, 4.5, 5.6 ms^{-1}) covering both the stable and the unstable forward speed range. Two individual trials were performed in random order for every speed. In one trial steering feedback was enabled (haptics on), whereas in the other trial steering feedback was reduced. The roll-steer dynamics were decoupled, hence the steering torque feedback was due to the inertia of the handlebars and not due to the front wheel dynamics (haptics off). Every trial had a duration of approximately 60 seconds, with on average a total of 12 lateral perturbations. Example data measured for one subject at the lowest speed is presented in Figure 2.

All experiments were performed at a straight cycling path at the Heertjeslaan on the TU Delft campus during the summer of 2019. The subjects were requested to ride the steer-by-wire bicycle at all four speeds while being laterally perturbed with impulsive forces at the seat post. An additional bicycle was used by the experiment coordinator to cycle next to the instrumented steer-by-wire bicycle and perturb the subject (see Figure 1(b)). A set-up which allowed both push and pulls was initially tested but the pushes were subject to inconsistencies. After inspecting the data of the pilot runs, it was observed that unilateral disturbances did not affect the predictability of the perturbation, as the responses of the
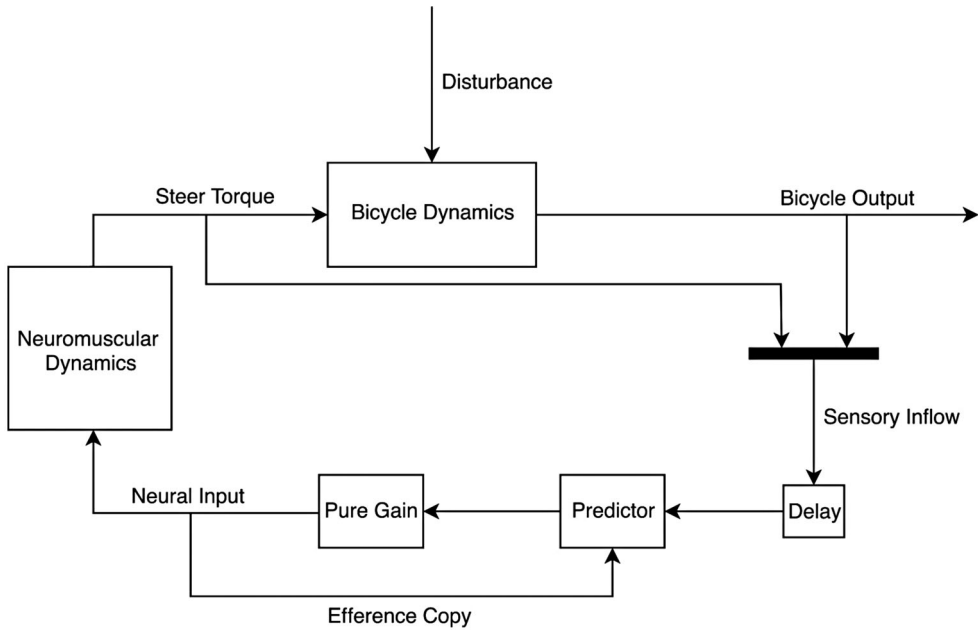
Figure 3. High level overview of the rider–bicycle model.

subjects were similar. For this reason, the unilateral approach was chosen. To avoid any feedforward control behaviour (e.g. seeing the coordinator preparing to pull the rope) all subjects were asked to focus on the road ahead.

3. System model

The present study builds upon the bicycle and rider model described by Schwab et al. [18] extending the rider model with neuromuscular dynamics and a predictor dealing with sensory delays (see Figure 3).

3.1. Bicycle model

We adopted the Carvallo–Whipple bicycle model [3] which consists of four rigid bodies: a rear frame B which includes the rider as a rigid mass with no hands on the handlebars, a front frame H which consists of the handlebar and fork assembly and a front wheel F (see Figure 10 in Appendix II – Bicycle and neuromuscular dynamics models). The bodies are connected with in total three revolute joints, one for each wheel and one for the steering axis connecting the rear and front frame. The contact between the wheels and the road surface is modelled by holonomic constraints in the normal direction and by non-holonomic constraints in the longitudinal and lateral directions with zero longitudinal and lateral slip. The resulting bicycle model has three velocity degrees-of-freedom, the forward speed v, the rear frame roll rate $\dot{\phi}$ and the steering rate $\dot{\delta}$.

Table 1. Sensory motor delays.

Bicycle states	Delay (ms)
δ	25
$\dot{\delta}$	25
T_δ	25
ϕ	200
ψ	200
$\dot{\phi}$	50

3.2. Rider control model

The rider inertia was integrated in the inertia of the bicycle rear frame B assuming a rigid connection to the saddle. In this paper we thereby ignore the contribution of body lean to balancing and steering (see the Section 6.1 and Appendix IV – Effects of rider body coupling analysed using a double pendulum model). The rider control model architecture consists of four main blocks in series (i.e. the sensory delay, the predictor, the linear gain controller and the neuromuscular dynamics) that represent human sensing, reasoning and actuation. The output states attributed to the proprioceptive, visual and vestibular system were delayed taking into account perception and neural delays presented in Table 1. For steering angle, steering velocity (muscle spindles) and steer torque (golgi tendon organs) delays were based on studies by Van der Helm et al. [28] and De Vlugt et al. [29] using similar linear second-order models to capture neuromuscular arm dynamics. For the roll and heading (yaw) angles we assumed visual perception with delays from Kawakami et al. [30], whereas for the roll rate, we assumed vestibular perception with a delay according to Barnett et al. [31].

A prediction algorithm which includes an internal model of the bicycle and neuromuscular dynamics was used to simulate how the central nervous deals with sensory delays and estimates the current state integrating applied control inputs. The predicted states were fed through the gain block which includes six free parameters (one for each bicycle state), estimated fitting the experimental data as described in the section *parameter estimation*. The produced neural control signal was filtered through the neuromuscular dynamics which gives as output the rider steer torque T_δ. The high level overview of the obtained rider–bicycle system can be seen in Figure 3.

3.3. Neuromuscular dynamics

To simulate the limitations of the rider's arm responses a linear second-order neuromuscular model was used similar to the approach adopted by Jason Moore in his PhD thesis [13]. The model uses activation dynamics estimated for the shoulder joint [32,33]. The model acts as a critically damped second-order filter with a cut-off frequency $\omega_c = 2.17 \cdot 2\pi$ rads^{-1} and damping coefficient $\zeta = \sqrt{1/2}$ generating the steer torque T_δ in reponse to the neural input a (see Appendix II – Bicycle and neuromuscular dynamics models).

3.4. *Sensory delay reafferent optimal predictor (SDROP)*

To compensate the effect of sensory delays and achieve an adequate rider control performance, we explored the use of internal predictive models. Several authors have proposed that the cerebellum functions as a predictor of body motion. Miall et al. [34] suggested that the cerebellum may hold at least two separate Smith Predictors. The Smith predictor is a basic prediction scheme in control theory [35]. The Smith predictor compensates for time delays using a forward model of the controlled dynamics and an internal model of the sensory delays. The forward model utilises an efferent signal being the applied neural control input a. The comparison between prediction and measurement simulates the human's ability to distinguish between reafference and exafference. Unfortunately, the Smith predictor does not work for unstable open loop systems [35] such as the Carvallo–Whipple bicycle model [3]. As a consequence, adjustments were made to the Smith predictor. The forward model was replaced by a discrete optimal predictor (DOP) which was adapted to work with different time delays Table 1. The more advanced sensory delay reafferent optimal predictor (SDROP) used additional delays to synchronise the input states and an internal model to forward the bicycle states in time. A comparison between the conventional DOP and the SDROP is presented in Figure 12 (a), (b) of Appendix III – Predictor comparison. The SDROP required full state feedback, but in our extended bicycle model only 6 out of 7 states are sensed. The missing $\dot{T}_\delta$ was estimated by the predictor. To detect disturbance effects, which are not captured by the efference copy, we utilised the same correction principle as used in the Smith predictor [35]. The low level overview of the rider controller and bicycle plant can be seen in Figure 4.

4. System identification

The rider control system identification used a combination of black box and gray box models to estimate the control gains employed by the rider. Starting with the basic measurements, the identification was performed in six steps:

(1) **Data preparation:** There were two datasets available for our analysis (haptics on and haptics off). An in depth comparison of these conditions is presented by Dialynas et al. [36]. The steering angle power spectrum was analogous with no significant effects on the power spectral centroid representing the frequency where most of the power is concentrated. Almost identical impulse response functions (IRFs) were reported. In haptics off the steering response was delayed around 20 ms for the three highest speeds ($p = 0.0021$ for 3.7 m/s, $p = 0.0001$ for 4.5 m/s, $p = 0.0002$ for 5.6 m/s) whereas no significant effect was found at 2.6 m/s. Given these minor experimental effects of haptic information, only the haptics on dataset was selected for modelling, and experimental trends will be adressed in the discussion. This dataset was split into two data clusters. The cluster with the first 10 subjects was used for 'identification' of the controller gains, and the cluster with the last 10 subjects for 'validation' of the model.
(2) **Black box identification:** To produce the filtered impulse response (IRF), finite impulse response (FIR) models were fitted to the four output states y in response to the lateral force w for each run.
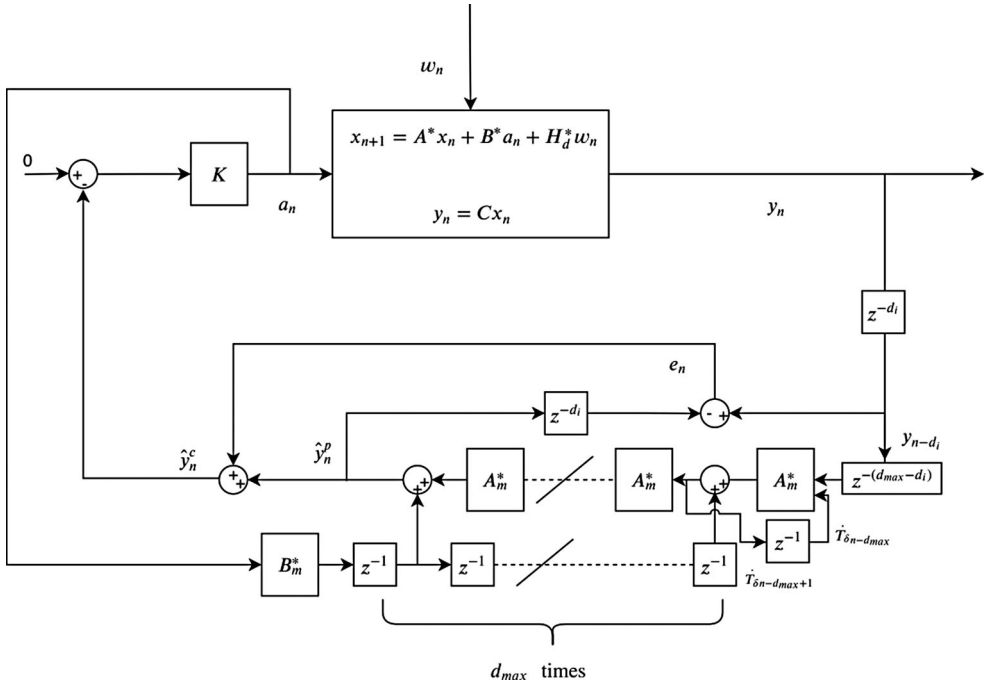
Figure 4. Low level overview of the rider–bicycle system. Matrices A^*, B^*, H^*_d are the discretised matrices of the extended plant dynamics, d_i is the amount of delay in times steps per sensory channel and d_{max} the maximum value of those. Matrices A^*_m, B^*_m express the dynamics of the internal model of the process. $\hat{y}^p$, $\hat{y}^c$ symbolise the undelayed and delayed estimates of the output states, respectively. e is the error between the predicted and delayed states (Smith correction) and K is a pure gain block containing all six gains. a represents the neural signal send to the rider arm muscles.

(3) **Filtering:** The IRFs h_δ (t), h_ϕ (t), h_ψ (t), h_{T_δ} (t) were filtered using a zero-phase low pass filter with a cut-off frequency of 10 Hz.

(4) **Median response:** The individual responses of the 'identification' and 'validation' datasets were averaged in order to produce two mean IRFs. Each individual subject response was compared with the mean. The subject with the best fit (highest VAF) for all runs was selected as the median rider for both datasets. We could also have used the two mean raw measurements to identify the median rider for the two aforementioned datasets but this was avoided due to the fact there was too much unwanted information in the experiments which was not directly attributed to the impulse perturbation. All results described herein were based on the median rider response IRFs, since intersubject variability was low at ±8%.

(5) **Black box filtering:** The IRFs of the median subject were convolved with the measured disturbances of each run to produce the non-parametric output states $\tilde{y}_\delta(t)$, $\tilde{y}_\phi(t)$, $\tilde{y}_\psi(t)$, $\tilde{y}_{T\delta}(t)$ $\tilde{y}_T$.

(6) **Gray box identification:** The rider control model with a maximum of six free parameters (one gain for each bicycle state feedback loop plus one for the steer torque) was fitted to the non parametric outputs $\tilde{y}_\delta$, $\tilde{y}_\psi \tilde{y}$ given the measured external input w.

These individual steps are explained in detail in the following sections.

4.1. Black box model

To remove unwanted disturbances and noise, the measured steering angle δ, roll angle ϕ, heading angle ψ and steer torque T_δ signals were approximated by a FIR model. The impulse response function $h(t)$ was convolved with the external input $w(t)$ to produce the filtered output response $\widetilde{y}(t)$. The output data represent the input to output relationship corresponding to either $h_\delta(t)$, $h_\phi(t)$, $h_\psi(t)$, $h_{T_\delta}(t)$. In finite discrete time; $t = 1, 2, 3\ldots, N$ the measured output $y(t)$ is given by,

$$y(t) = \widetilde{y}(t) + v(t) \tag{1}$$

$$\widetilde{y}(t) = \sum_{k=1}^{m} h(k)w(t - k) \tag{2}$$

where m is the sample length of the impulse response function and $v(t)$ is the remnant caused by the unwanted disturbances. Experimenting with different finite impulse lengths, the oscillations were found to die out after $m = 798$ samples, which corresponds to a finite response length of 3.08 seconds. In state space form Equations (1), (2) are expressed as,

$$y = Wh + v \tag{3}$$

where W is the matrix containing time shifted versions of the input signal.

$$W = \begin{bmatrix} w(0) & 0 & 0 & \ldots & 0 \\ w(1) & w(0) & 0 & \ldots & 0 \\ w(2) & w(1) & w(0) & \ldots & 0 \\ \vdots & \vdots & \vdots & \ddots & 0 \\ w(N-1) & w(N-2) & w(N-3) & \ldots & w(N-N) \end{bmatrix} \tag{4}$$

Since Equation (3) is linear in the coefficients a unique solution can be found by the least squares method.

$$h = \left(W^T W \right)^{-1} W^T y \tag{5}$$

The estimated IRFs were further filtered using a eight-order Butterworth filter with cut-off frequency of 10 Hz. All input signals were convolved with h in order to remove noise and produce an estimate of the output signals $\widetilde{y}$. An example of obtained responses of the mean and median rider for the lowest measured forward velocity is presented in Figure 5.

4.2. Gray box model

The rider control model includes six unknown linear feedback control gains. In state space the gain block of Figure 4 can be expressed as a vector of the following form, $\mathbf{K} = [K\dot{\phi}, K\dot{\delta}, K_\phi, K_\delta, K_\psi, K_{T_\delta}]^T$.

As feedback is defined as negative, the control input is given by:

$$a = -\mathbf{K}\hat{\mathbf{y}}^c \tag{6}$$

where $\hat{\mathbf{y}}^c$ is the output of the predictor (see Figure 3).
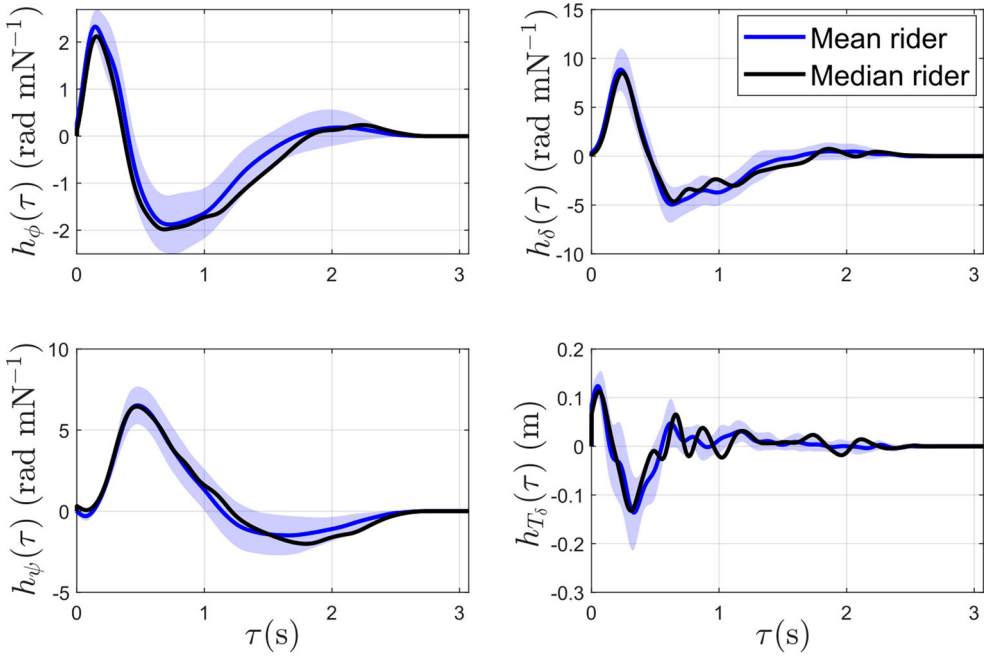
Figure 5. IRFs for the roll angle ϕ, steering angle δ, heading angle ψ and steer torque T_δ for a forward velocity of $v = 2.8ms^{-1}$, shade $=$ SD of mean over participants (haptics on).

4.3. Parameter estimation

The gains of the rider control model were estimated by fitting the model outputs into the convolved filtered IRFs. This was achieved minimising the following cost function:

$$
V_N(\mathbf{K}) = \frac{1}{N} \sum_{t=1}^{N} \left[0.8 \frac{\left(\hat{y}_\delta(t, \mathbf{K}) - \widetilde{y}_\delta(t) \right)^2}{\left(\bar{y}_\delta \right)^2} \right.
$$

$$
\left. + 0.16 \frac{\left(\hat{y}_\psi(t, \mathbf{K}) - \widetilde{y}_\psi(t) \right)^2}{\left(\bar{y}_\psi \right)^2} + 0.04 \frac{\left(\hat{y}^{T_\delta}(t, \mathbf{K}) \right)^2}{\left(\bar{y}_{T_\delta} \right)^2} \right] \tag{7}
$$

where $\mathbf{K}$ is a vector containing all free feedback control gains and $\hat{y}_\delta$, $\hat{y}_\psi$ and $\widetilde{y}_\delta(t), \widetilde{y}_\psi(t)$, are the simulated and non-parametric outputs, respectively. The constant scaling factors $\bar{y}_\delta$, $\bar{y}_\psi$ and $\bar{y}_{T\delta}$ are the absolute allowable magnitude limits, which are 0.4 rad for the two angles and 10 Nm for the steering torque.

The first two terms of the cost function are trying to match the steering and heading responses of the parametric model with the non-parametric model. The third term minimises the magnitude of input torque in order to optimise fitting, while minimising the control effort. Omission of this term led to oscillatory steering angles and unrealistic input torques, due to the double differentiation to get from position to torque. Roll responses were not fitted due to systematic deviations between the predicted and actual responses (see Section 6.1 in the 6). All weights of the cost function were chosen heuristically, the

weight ratio of the heading and steer error was selected as 1:5, since this gave the best fit. For optimisation a genetic algorithm (fitness limit = 0.03, crossover fraction = 0.85, and population size = 10 times bigger the size of the parameter length) was used followed by a gradient descend algorithm to estimate the global minimum of the gains.

Most estimated gains of the rider model were negative, producing torques opposed to the state direction. Due to the fact that the rider was expected to act like a restoring steering stabiliser with finite stiffness and damping properties, all gains associated to the arm muscle spindles (K_δ, $K_{\hat\delta}$) were constrained to be only positive. At the same time, the heading and roll gains (K_ψ, K_ϕ) were constrained between -250 and 250 kg m^2 s^{-1}, because if they were left unconstrained they drove the gain vector to unrealistic values without noticeable improvement in fitting performance.

4.4. Performance metrics

As metric of model validity the variance accounted for between the parametric and non-parametric output was calculated as,

$$\text{VAF}_d(\mathbf{K}) = 1 - \sum_{t=1}^{N} \left(\widetilde{y}_d(t) - \hat{y}_d(t, \mathbf{K}) \right)^2 / \sum_{t=1}^{N} \left(\widetilde{y}_d(t)^2 \right) \tag{8}$$

with d being any of the roll ϕ, steer δ and heading ψ outputs. To quantify the uncertainty of each parameter the covariance matrix was first estimated as,

$$\text{cov}_{ij}(\hat{\mathbf{K}}) = V_N(\hat{\mathbf{K}}) H_{ij}(\hat{\mathbf{K}})^{-1} \tag{9}$$

where the hessian matrix $\mathbf{H}$ was calculated by the gradient descend algorithm as,

$$\mathbf{H}(\hat{\mathbf{K}}) = H_{ij}(\hat{\mathbf{K}}) = \frac{\partial^2 V_N}{\partial K_i \partial K_j} \tag{10}$$

where $\hat{\mathbf{K}}$ in both Equations (9), (10) stands for the closest estimate to the true parameter vector $\mathbf{K}^*$, that produces the true global minimum. To obtain comparable results between the estimated parameters the diagonal elements of the covariance matrix $\text{cov}_{ij}(\hat{K})$ were normalised with the respective parameter estimate. The normalised coefficient of variation for each parameter was calculated as,

$$CV_i = \sqrt{\frac{\sigma_{\hat{K}_i}^2}{\hat{K}_i^2}} \tag{11}$$

where $\sigma_{\hat{K}_i}^2$ stands for the diagonal elements in this equation.

5. Results

Three rider models with increasing complexity are presented and discussed in this Section (1) A zero delay (ZD) model which ignores sensory delays and hence the bicycle states are direct inputs to the Pure Gain block (see Figure 3), (2) a model with sensory delays

(SD) (see Table 1) but without predictor, and (3) a model with sensory delays and reafferent optimal predictor (SDROP). The performance of all models is assessed for three different configurations. In the first and presumably most realistic configuration (with T_δ feedback) the rider has the torque feedback loop connected and the plant dynamics approximate a normal bicycle. In the second configuration (without T_δ feedback) the internal torque feedback loop of the rider is disconnected (hence there are 5 instead of 6 feedback parameters). This will show in how far a human control model *without steering torque feedback* can explain normal human behaviour. In the third configuration (reduced T_δ feedback) the steering dynamics change to steer-by-wire (haptics off). This means that the plant approximates a bicycle with decoupled roll-steer dynamics, hence the rider receives only steering torque feedback due to the inertia of the handlebars and not due to the front wheel dynamics. This will show in how far a human control model with *reduced steering torque feedback* information can explain normal human behaviour.

Results showed that all rider models followed the necessary stability condition of steer into the fall and were capable of stabilising the bicycle. This is illustrated in Figure 6 comparing all models and configurations for the lowest and highest measured speeds. Rider model parameters and the model fit (VAF) for all models and configurations are reported in detail in Tables 2–4. Figure 7 illustrates the model fit for the three rider models for the configuration with torque feedback. All rider models provide reasonable or good fits of the steering and heading angle. The roll angle is not so well predicted where the magnitude of the roll angle remains two to three times smaller than the actual non-parametric output, as will be further addressed in Section 6.1 in the 6. The model without sensory delays (ZD) provides a good overall fit, while the fit degraded introducing sensory delays (SD) and improved with the advanced SDROP model where the Smith predictor compensates for sensory delays. Rider control parameters vary strongly with driving speed for all models and configurations as illustrated in Figure 8. The hypothesis was that the absolute value of the K_ψ will increase with speed and K_δ will decrease as we also noticed in our analysis. Our expectations were based on subjective observations from other naturalistic bicycle studies. As a conclusion we believe that the rider uses more the relevant position of the handlebars (proprioceptive cues) at lower speeds. At higher speeds the heading of the bicycle (visual cues) plays a more significant role when the subject is laterally perturbed.

5.1. Zero delay (ZD)

The results of the zero delay model for all configurations and speed levels are presented in Table 2. A VAF of over 90% was observed for both the steer angle and heading, while for the roll angle the VAF is between 77–90% depending on speed and configuration. The CV indicates moderate dispersion for most gains and speed levels, except for the w/o T_δ configuration where the uncertainty of K_δ is much higher than the rest of the gains. For all speed levels VAF_δ drops the most in the w/o T_δ feedback configuration. The steering angle and torque signals become substantially more oscillatory, although roll stabilisation does not seem to be affected. With reduced T_δ feedback, VAF_δ drops less than 3% and the degradation in the steering angle, torque and roll signals is small. All model predictions lag behind compared to the non-parametric responses. For the roll angle the predicted magnitude is two to three times smaller than the measured output.
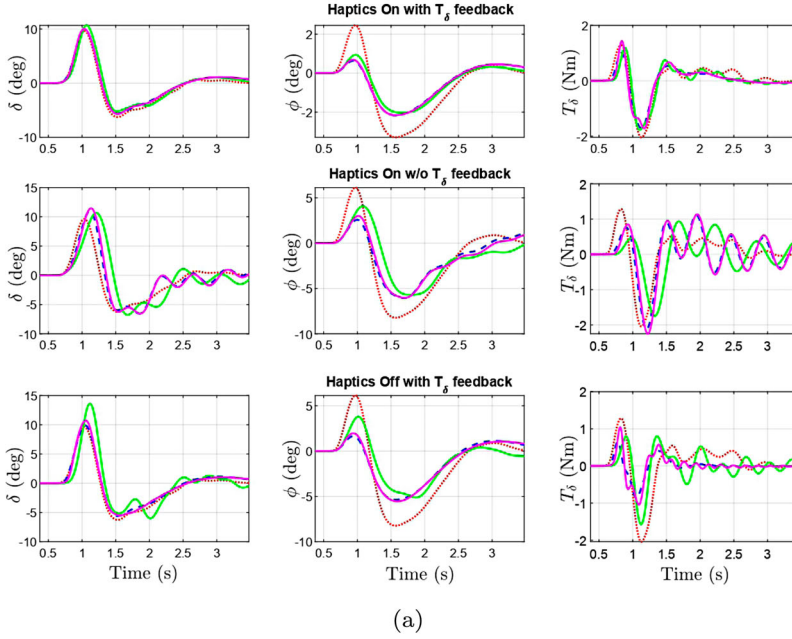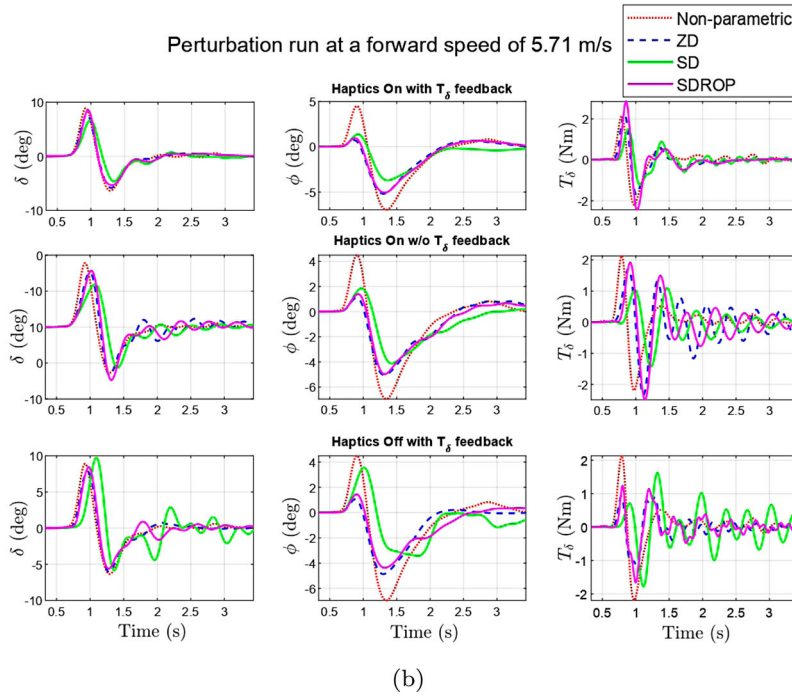
Figure 6. Steering angle δ, roll angle ϕ and steering torque T_δ of the three parametric rider models (ZD, SD, SDROP) compared to the Non-parametric model, for all torque feedback configurations, for the lowest speed (top) and highest speed (bottom).
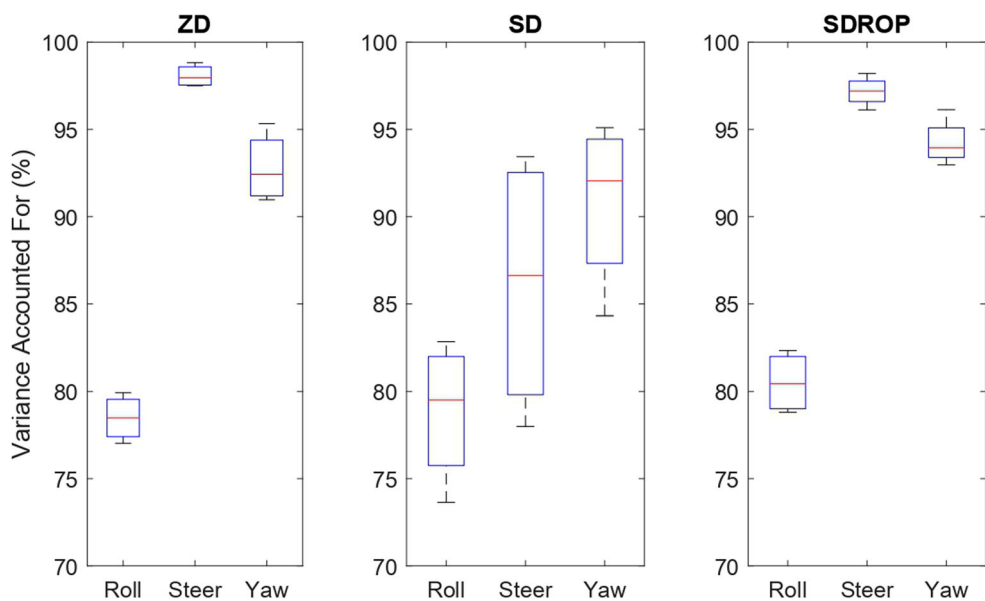
Figure 7. Variance accounted for (VAF) for rider models with zero delay (ZD-left), with sensory delay (SD, middle), and sensory delay reafferent optimal predictor (SDROP-right). In all cases the VAF is shown averaged over 4 speeds for rider models with torque feedback. Detailed results are presented in Tables 2–4.
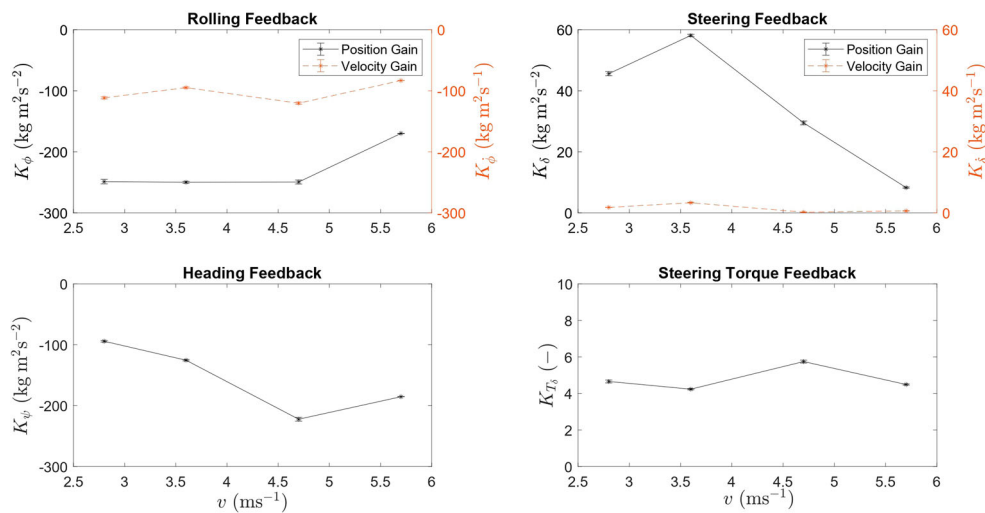
Figure 8. Rider control parameters as a function of riding speed for the most advanced SDROP model with force feedback, bars indicate the coefficient of variance (CV) indicating the parameter estimation accuracy. Control parameters for all rider models are in Tables 2–4.

5.2. With sensory delay (SD)

The results of the sensory delay model for all configurations and speed levels are presented in Table 3. The model fit degraded by the introduction of sensory delays. The model with

Table 2. Results of the zero delay (ZD) model for the median rider for all configurations and speed levels.

		Haptic On				Haptic Off	
		with T_δ feedback		w/o T_δ feedback		reduced T_δ feedback	
	Bicycle model						
Speed	Rider model	Value	CV (10^{-4})	Value	CV (10^{-4})	Value	CV (10^{-4})
	$K_{\dot\phi}$	−77.17	114.86	−22.46	29.77	−115.36	213.52
2.8 ms^{-1}	$K_{\dot\delta}$	2.26	73.57	2.58	18.93	8.76	187.30
	K_ϕ	−164.88	132.25	−24.50	73.14	−248.24	217.05
	K_δ	32.75	150.14	3.76	140.96	29.67	215.07
	K_ψ	−63.22	133.29	−9.85	53.71	−93.44	223.02
	K_{T_δ}	3.51	176.20	–	–	7.53	223.83
	VAF_ϕ	77.80		82.79		78.37	
	VAF_δ	98.34		79.19		98.20	
	VAF_ψ	93.46		93.51		93.74	
	$K_{\dot\phi}$	−109.94	146.98	−21.30	35.99	−78.28	61.00
3.6 ms^{-1}	$K_{\dot\delta}$	8.22	139.00	3.30	24.78	9.09	51.11
	K_ϕ	−248.47	147.39	−34.64	71.54	−229.14	84.40
	K_δ	50.78	147.72	6.48	130.57	53.16	92.96
	K_ψ	−132.13	152.08	−17.74	61.92	−103.75	74.49
	K_{T_δ}	4.52	167.24	–	–	6.89	64.17
	VAF_ϕ	79.92		85.93		80.89	
	VAF_δ	98.83		86.40		97.08	
	VAF_ψ	95.33		97.95		95.15	
	$K_{\dot\phi}$	−92.50	117.34	−27.29	46.40	−102.63	40.87
4.7 ms^{-1}	$K_{\dot\delta}$	4.81	183.05	4.25	41.56	11.24	28.38
	K_ϕ	−183.03	135.64	−38.17	76.43	−249.74	74.10
	K_δ	22.57	237.51	2.65	591.87	63.36	88.33
	K_ψ	−165.42	126.89	−33.78	63.74	−188.67	58.81
	K_{T_δ}	3.42	174.23	–	–	8.98	13.88
	VAF_ϕ	77.03		83.06		78.60	
	VAF_δ	97.57		80.27		95.57	
	VAF_ψ	91.41		97.03		92.48	
	$K_{\dot\phi}$	−83.90	117.61	−31.12	43.99	−76.30	47.12
5.7 ms^{-1}	$K_{\dot\delta}$	5.83	142.87	5.58	40.62	10.91	30.23
	K_ϕ	−166.08	127.89	−43.64	67.14	−208.33	83.09
	K_δ	14.85	98.10	1.14	1836.39	79.44	75.47
	K_ψ	−186.77	128.56	−49.82	52.31	−176.96	69.82
	K_{T_δ}	3.24	185.07	–	–	8.45	29.67
	VAF_ϕ	79.17		84.03		80.30	
	VAF_δ	97.51		84.09		94.71	
	VAF_ψ	90.97		96.41		91.56	

Notes: Haptic on/off differentiates based on the dynamics of the bicycle model, while 'with or w/o T_δ feedback' differentiates based on the structure of the rider control model. The values of the gains are presented together with their corresponding uncertainty level (CV). The VAF between the parametric and non-parametric signal outputs is also presented in percentage % to assess fitting performance. The derivative gains $K_{\dot\phi}$, $K_{\dot\delta}$ are measured in $\mathrm{kg\,m^2\,s^{-1}}$, the proportional gains K_ϕ, K_δ, K_ψ are measured in $\mathrm{kg\,m^2\,s^{-2}}$ and the torque feedback gain K_{T_δ} is dimensionless.

normal steering torque feedback provided a reasonable fit but VAF_δ dropped, in particular for higher speeds (from 97.5% to 78% at 5.7 ms^{-1}). The CV indicates moderate dispersion for most gains and speed levels, except for the steer angle gain K_δ, where a higher dispersion was observed for the highest speeds. In contrast to the previous model a larger drop in the VAFs of all signals was observed between the first two configurations (with and w/o T_δ feedback), and an equally significant further drop with reduced T_δ feedback. The additional delay was also evident in the predicted signals (see Figure 6). The magnitude of the roll angle remains two to three times smaller than the actual non-parametric output.

Table 3. Results of the with sensory delay (SD) model for the median rider for all configurations and speed levels.

| | | Haptic On | | | | Haptic Off | |
| | | with T_δ feedback | | w/o T_δ feedback | | reduced T_δ feedback | |
Speed	Rider model	Value	CV (10^{-4})	Value	CV (10^{-4})	Value	CV (10^{-4})
2.8 ms^{-1}	$K_{\dot\phi}$	−68.53	38.72	−14.93	37.52	−28.19	35.15
	$K_{\dot\delta}$	2.09	110.32	2.30	32.17	2.65	13.18
	K_ϕ	−146.29	72.07	−16.98	92.51	−79.20	78.41
	K_δ	22.18	95.38	4.62	103.75	10.51	93.36
	K_ψ	−40.34	56.18	−3.78	116.84	−14.53	67.08
	K_{T_δ}	3.52	64.80	–	–	2.59	29.48
	VAF_ϕ	81.15		69.61		80.01	
	VAF_δ	93.43		23.34		66.84	
	VAF_ψ	93.78		69.67		83.30	
3.6 ms^{-1}	$K_{\dot\phi}$	−51.02	56.62	−15.40	55.90	−21.25	51.31
	$K_{\dot\delta}$	2.50	170.45	2.81	50.20	2.79	17.72
	K_ϕ	−120.51	85.28	−22.82	102.83	−76.41	90.89
	K_δ	16.58	153.27	3.94	243.76	17.14	84.92
	K_ψ	−43.06	79.41	−7.37	147.32	−13.30	103.52
	K_{T_δ}	3.42	62.79	–	–	3.09	21.20
	VAF_ϕ	82.85		79.48		73.14	
	VAF_δ	91.63		53.29		52.83	
	VAF_ψ	95.10		84.88		71.58	
4.7 ms^{-1}	$K_{\dot\phi}$	−51.78	64.60	−19.26	349.70	−14.88	55.92
	$K_{\dot\delta}$	2.75	160.68	4.42	438.96	3.04	20.62
	K_ϕ	−136.22	105.15	−27.02	111.78	−48.91	115.90
	K_δ	3.21	1156.00	0.01	492609.67	16.01	99.26
	K_ψ	−64.43	87.60	−14.29	412.99	−10.82	119.48
	K_{T_δ}	3.70	63.91	–	–	2.61	30.62
	VAF_ϕ	77.86		71.14		63.73	
	VAF_δ	81.63		36.19		15.61	
	VAF_ψ	90.32		80.57		55.71	
5.7 ms^{-1}	$K_{\dot\phi}$	−38.58	136.91	−19.65	110.85	−10.10	62.29
	$K_{\dot\delta}$	1.13	2085.75	5.42	128.32	3.08	21.38
	K_ϕ	−120.59	120.57	−33.34	117.63	−30.95	133.76
	K_δ	0.00	3969013.40	0.01	280859.33	18.46	79.69
	K_ψ	−60.65	95.03	−19.20	183.00	−8.17	131.56
	K_{T_δ}	4.27	191.50	–	–	2.58	26.58
	VAF_ϕ	73.65		70.08		49.58	
	VAF_δ	77.99		40.64		–	
	VAF_ψ	84.32		79.50		39.90	

Notes: Haptic on/off differentiates based on the dynamics of the bicycle model, while 'with or w/o T_δ feedback' differentiates based on the structure of the rider control model. The values of the gains are presented together with their corresponding uncertainty level (CV). The variance accounted for (VAF) between the parametric and non-parametric signal outputs is also presented in percentage % to assess fitting performance. The derivative gains $K_{\dot\phi}$, $K_{\dot\delta}$ are measured in kg m^2 s^{-1}, the proportional gains K_ϕ, K_δ, K_ψ are measured in kg m^2 s^{-2} and the torque feedback gain K_{T_δ} is dimensionless.

5.3. Sensory delay reafferent optimal predictor (SDROP)

The results of the SDROP model for all configurations and speed levels are presented in Table 4. Despite the fact that significant delays are introduced into the sensory paths Table 1 the internal model of the predictor compensates for system latencies and achieves a good performance for all three configurations. A VAF above 90% was observed for both the steer angle and heading, while for the roll angle VAF is between 80–86% depending on speed and configuration. The CV indicates a stable level of dispersion for most gains and speed levels. Only for the configuration with T_δ feedback a higher dispersion was observed for

Table 4. Results for the SDROP model for the median rider for all configurations and speed levels.

		Haptics On				Haptics Off	
		with T_δ feedback		w/o T_δ feedback		reduced T_δ feedback	
	Bicycle model						
Speed	Rider model	Value	CV (10^{-4})	Value	CV (10^{-4})	Value	CV (10^{-4})
2.8 ms^{-1}	$K_{\dot\phi}$	−111.62	152.10	−22.44	28.45	−123.53	27.90
	$K_{\dot\delta}$	1.80	234.11	2.62	14.59	8.62	35.62
	K_ϕ	−248.74	151.15	−24.17	84.44	−239.60	18.65
	K_δ	45.60	150.24	4.05	147.97	22.82	90.52
	K_ψ	−94.18	156.50	−9.03	65.63	−91.07	14.16
	K_{T_δ}	4.66	170.99	–	–	7.93	27.78
	VAF_ϕ	78.80		82.33		80.67	
	VAF_δ	98.21		68.99		97.59	
	VAF_ψ	94.04		90.77		94.95	
3.6 ms^{-1}	$K_{\dot\phi}$	−94.83	125.80	−22.08	33.58	−97.15	115.92
	$K_{\dot\delta}$	3.33	404.51	3.34	17.01	9.68	75.60
	K_ϕ	−249.80	64.02	−37.61	80.02	−249.84	214.29
	K_δ	58.12	63.15	7.44	140.22	50.23	247.35
	K_ψ	−125.36	97.89	−17.72	66.95	−119.20	160.68
	K_{T_δ}	4.24	91.84	–	–	7.57	95.88
	VAF_ϕ	81.66		86.50		83.35	
	VAF_δ	97.33		79.27		96.15	
	VAF_ψ	96.13		96.97		96.80	
4.7 ms^{-1}	$K_{\dot\phi}$	−120.38	145.55	−27.59	56.00	−164.59	112.31
	$K_{\dot\delta}$	0.24	4252.46	4.15	59.72	22.39	106.46
	K_ϕ	−249.40	133.42	−37.98	90.28	−249.82	107.93
	K_δ	29.49	210.73	2.67	665.03	14.70	649.60
	K_ψ	−222.31	143.06	−31.24	81.57	−209.12	111.47
	K_{T_δ}	5.75	141.98	–	–	13.87	78.12
	VAF_ϕ	79.21		81.88		80.97	
	VAF_δ	97.07		70.43		90.44	
	VAF_ψ	92.97		95.43		95.93	
5.7 ms^{-1}	$K_{\dot\phi}$	−83.24	24.27	−27.53	46.08	−146.38	35.81
	$K_{\dot\delta}$	0.65	1394.64	4.31	43.06	28.45	31.76
	K_ϕ	−169.81	13.03	−44.71	92.82	−246.85	116.80
	K_δ	8.29	278.33	4.13	493.77	29.42	401.88
	K_ψ	−185.36	6.72	−43.34	72.02	−211.40	56.88
	K_{T_δ}	4.49	72.85	–	–	15.81	10.28
	VAF_ϕ	82.35		85.06		80.57	
	VAF_δ	96.12		75.40		87.27	
	VAF_ψ	93.83		97.03		93.59	

Notes: Haptic on/off differentiates based on the dynamics of the bicycle model, while 'with or w/o T_δ feedback' differentiates based on the structure of the rider control model. The values of the gains are presented together with their corresponding uncertainty level (CV). The variance accounted for (VAF) between the parametric and non-parametric signal outputs is also presented in percentage % to assess fitting performance. The derivative gains K_ϕ, K_δ are measured in $\mathrm{kg\,m^2\,s^{-1}}$, the proportional gains K_ϕ, K_δ, K_ψ are measured in $\mathrm{kg\,m^2\,s^{-2}}$ and the torque feedback gain K_{T_δ} is dimensionless.

the steer rate $K_{\dot\delta}$ and steer angle gains K_δ. A drop in VAF_δ and an oscillatory behaviour similar to the ZD model was observed in the w/o T_δ and reduced T_δ configurations. Also for this model the predicted roll angle magnitude remains two to three times smaller than the actual non-parametric output.

5.4. Testing and validation

The SDROP prediction capabilities are also tested without the Smith correction control loop, testing the performance of the simpler DOP (see Figure 12 of Appendix III – Predictor

comparison). To simplify the comparison the gain estimates of the ZD model are adopted for both SDROP and DOP simulations. A comparison between the true roll rate and predicted roll rate of the DOP and SDROP model without any internal model discrepancies is presented in Figure 9(a). The state estimate of the SDROP model is closest to the true state, which is expected since the Smith loop corrects the error between the state estimates by comparing its predicted states with the direct outputs of the bicycle model. However, the main advantage of the Smith correction loop is the ability to correct for internal model imperfections, which come along with changes in the bicycle plant dynamics.

To examine this ability the forward model of the SDROP is replaced with that of the configuration with reduced T_δ feedback. This is based on the assumption that the rider has a reduced perception of bicycle dynamics when riding the steer-by-wire bicycle in the haptics off configuration. A comparison between the true roll rate and predicted roll rate of the DOP and SDROP with internal model imperfections is presented in Figure 9(b). The SDROP manages to handle all model imperfections with high performance, while the DOP predictions are oscillatory and lag behind compared to the true state estimates.

All results presented up to now, included feedback of steering angle and steering angle rate. To assess the importance of these loops, we also simulated the SDROP model omitting either or both feedback loops. Results in Table 5 (see Appendix V – Additional tables) demonstrated a poor fit for the highest speeds, in particular when removing both feedback loops. More specifically, VAF_δ dropped from approximately 90 to 60%, VAF_ϕ dropped from 80 to 26% and VAF_ψ dropped from 94 to 20%.

As a final step the simulated outputs of the SDROP model, which derive from the modelling dataset, are compared with the non-parametric responses of the validation dataset. The resulting VAFs are summarised in Table 6 (see Appendix V – Additional tables). Even though the perturbations in the validation set occurred at slightly lower speeds than the modelling dataset, most estimated VAFs are inline with those presented in the aforementioned tables. The median rider responses obtained from the two datasets lead to similar simulated responses and VAFs. To that end, all results described herein are justified indicating high quality of the identified rider models.

6. Discussion

Experiments with a steer-by-wire bicycle and human rider models were used to investigate human controlled bicycle balance and steering. The experiment explored the role of haptic steering torque feedback and the rider models captured this dataset with feedback loops for visuo/vestibular motion, steering torque, and steering angle feedback while taking into account sensory delays. The experiment showed marginal effects of haptic steering torque feedback on steering actions and bicycle motion. The rider models confirm that human bicycle control can indeed be captured by a rider model without steering torque feedback. This aligns with earlier models providing a good fit with rider models without torque feedback for treadmill and gymnasium data [13] and for treadmill data [18]. However our models showed the best performance for the haptics on with T_δ feedback configuration, with a VAF mostly over 90% for all speeds. Torque feedback gains could be estimated with good accuracy supporting the relevance of torque feedback. The absence of clear experimental effects of torque feedback can be explained by the model with reduced T_δ feedback which is equivalent to the experimental haptics off condition. This feedback
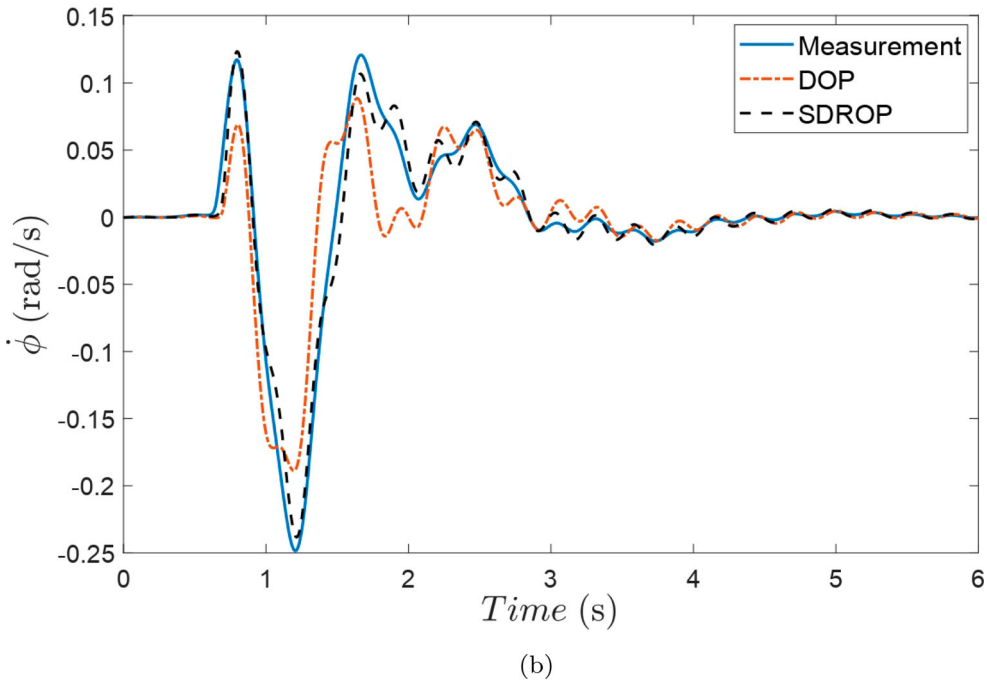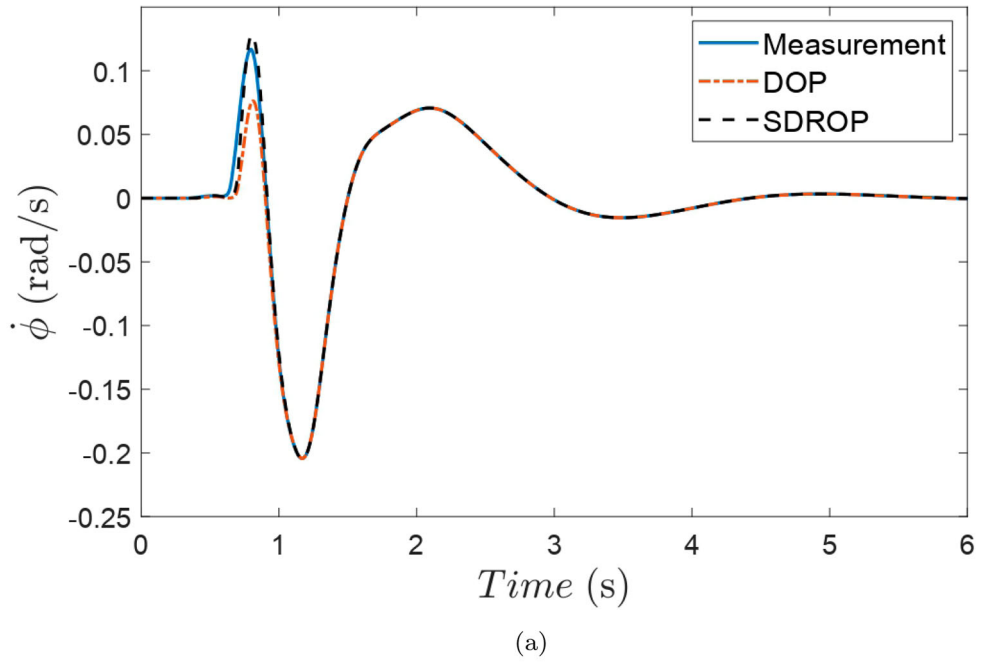
Figure 9. Comparison of true roll rate with simulated response of the DOP and SDROP predictors, (a) without internal model imperfections, (b) with internal model imperfections.

only senses muscular torques acting on the steer inertia and does not sense any moments resulting from bicycle dynamics including wheel inertia and road/tire interaction. Hence, we tend to conclude that torque feedback is relevant but not dominant in bicycle balance

and steering in the conditions studied. We focused on stabilisation on a straight and flat bicycle lane and haptic steering torque may well be more relevant in other conditions.

Earlier models ignored sensory delays [13,18]. We investigated the role of sensory delays using three control models varying presence of delays (ZD vs. SD) and prediction (SDROP). Comprehensive analysis of the three control models indicated almost identical responses between the ZD and SDROP models. The minor differences between ZD and SDROP can be explained as follows. The predictor can accurately estimate effects of steering actions (efference copy) but only detects effects of external perturbations after the sensory delay. This explains the small time delay between 20 and 80 ms observed in the predictions of the SDROP model. The SD model responses were more strongly delayed compared to the actual measurements, with a delay between 20 and 120 ms, due to sensory delays and missing prediction capabilities, resulting in a reduced fit of the experimental data. For the SDROP model omitting both steering angle δ and steering rate $\dot{\delta}$ had a negative effect on the fitting performance especially for the highest speeds. A large drop of about 70% was evident for VAF_ψ with a drop of about 50% for VAF_ϕ and a drop of about 20% for VAF_δ. The higher degradation of the heading and roll VAFs indicates that handlebar position and velocity feedback (muscle spindles) enhance bicycle heading and roll control at higher speeds.

The gains for roll K_ϕ, $K_{\dot{\phi}}$ and heading K_ψ are consistently negative for all models, configurations and speeds. This is in full agreement with the basic bicycle balance mechanism: to steer into the direction of the undesired fall [4]. The heading gain K_ψ exhibits a consistent trend, its magnitude increases with speed. This means that at higher speeds the rider focus is shifted towards heading control.

6.1. Limitations and outlook

Neuromuscular dynamics of the arms in steering were described by a linear second-order low pass filter in line with [28,29,32,33,37,38]. Feedback gains of the resulting steering angle, steering velocity and steering torque were estimated and these three proprioceptive feedback loops contributed to the fit of the experimental data supporting their relevance in bicycle control. Non-linear Hill type muscle models separating agonist and antagonist muscle groups can enhance model realism and allow study of muscular co-contraction stiffening the arms, and compliance of hand to steering wheel contact and effects of arm inertia can be explored [39]. Explicit modelling of cocontraction could separate intrinsic from reflexive arm stabilisation. However, the additional parameters introduced by more complex neuromuscular models, and their variation with task [29,37,38] will complicate rider model parameter estimation and would ideally be supported by more advanced measurements and perturbations, for instance perturbing the steering wheel in line with studies on the arm [28,29,32,33,37,38] and car steering [39].

We now assumed visual perception of body rotation in roll and yaw (heading) and vestibular perception of body roll rate. These three motion feedback loops were essential to obtain realistic results. Model realism can be enhanced integrating models of sensory integration combining visual motion perception with vestibular perception of rotational velocity by the semicircular canals and of acceleration combined with graviception by the otoliths [40,41]. Such models use state estimation techniques and could be integrated with predictors like the SDROP presented in this paper to deal with sensory delays.

For all models the predicted magnitudes of the roll angle remained two to three times smaller than the actual measured output (see Figure 6). During the experiments the upper body remained unconstrained and acted as a double inverted pendulum with some torsional spring and damping properties capturing lumbar bending and pelvis rotation. Additional simulations with a passive pendulum model showed a much higher roll angle of the bicycle when the rider is more compliant (see Figure 13 of Appendix IV – Effects of rider body coupling analysed using a double pendulum model). Such additional degrees of freedom need further study measuring upper body kinematics and exploring passive and active body stabilisation models, including rider control strategies using body lean to steer and balance.

7. Conclusion

A dataset perturbing balance on a straight bicycle lane was collected and used to develop rider-control models at four driving speeds. In an effort to iterate over existing rider-control models, a sensory delay reafferent optimal predictor model (SDROP) model has been created that successfully accounts for sensory delays by the use of an internal forward model. The sensory delay (SD) model has proven that implementation of sensory delays without feedforward compensation does not produce results that match the experimental data. A prediction strategy has been developed that manages to circumvent the inability of the conventional Smith predictor to work on inherently unstable open loop systems. The rider model is able to control the bicycle at all speeds and follows the necessary stability condition of steer into the fall. All simulated responses match the non-parametric outputs with high level of performance, even when internal model inaccuracies are introduced.

With this rider model the importance of accurate determination of the various state variables via our body sensors has been examined. The analysis showed that a highly realistic rider model besides lean angle, and lean velocity, must include steer angle, steer velocity and torque feedback to obtain adequate performance at all speed levels. However, if the torque feedback loop is severed and not disconnected as in the haptics off configuration, state information might be deduced from the other state variables.

Data availability

All the data used in this manuscript are available online at https://doi.org/10.5281/zenodo.5818396 (Dialynas et al., 2019).

Disclosure statement

The authors declare that they have no conflict of interest.

ORCID

Georgios Dialynas http://orcid.org/0000-0002-6857-0320
Riender Happee http://orcid.org/0000-0001-5878-3472
A.L. Schwab http://orcid.org/0000-0001-5897-9790

References

[1] Schwab AL, Meijaard JP. A review on bicycle dynamics and rider control. Veh Syst Dyn. 2013;51(7):1059–1090.

[2] Borrell B. Physics on two wheels. Nature. 2016;535(7612):338–341.

[3] Meijaard JP, Papadopoulos JM, Ruina A, et al. Linearized dynamics equations for the balance and steer of a bicycle: a benchmark and review. Proc R Soc A: Math, Phys Eng Sci. 2007;463(2084):1955–1982.

[4] Kooijman JDG, Meijaard JP, Papadopoulos JM, et al. A bicycle can be self-stable without gyroscopic or caster effects. Science. 2011;332(6027):339–342.

[5] Schepers P, Wolt KK. Single-bicycle crash types and characteristics. Cycling Res Int. 2012;2(1):119–135.

[6] Bulsink VE, Kiewiet H, van de Belt D, et al. Cycling strategies of young and older cyclists. Hum Mov Sci. 2016;46:184–195.

[7] McRuer DT, Krendel ES. The human operator as a servo system element. J Franklin Inst. 1959;267(5):381–403.

[8] McRuer DT, Graham D, Krendel ES. Manual control of single-loop systems: part I. J Franklin Inst. 1967;283(1):1–29.

[9] Van Lunteren A, Stassen H, Schlemper M. On the influence of drugs on the behavior of a bicycle rider. Proceedings of the 6th Annual Conference on Manual Control; OH, USA: Wright Patterson AFB; p. 7–9.

[10] Weir DH. A manual control view of motorcycle handling. Tech. Rep., 1973.

[11] Sharp RS. The stability and control of motorcycles. J Mech Eng Sci. 1971;13(5):316–329.

[12] Eaton D. Man-machine dynamics in the stabilization of single-track vehicles [PhD thesis]. University of Michigan; 1975.

[13] Moore JK. Human control of a bicycle [PhD thesis]. Davis (CA): University of California Davis; 2012 Aug.

[14] Hess R, Moore JK, Hubbard M. Modeling the manually controlled bicycle. IEEE Trans Syst, Man, and Cybern-Part A: Syst Humans. 2012;42(3):545–557.

[15] Soudbakhsh D, Zhang Y, Yi J. Stability analysis of human rider's balance control of stationary bicycles. 2012 American Control Conference (ACC); IEEE; p. 2755–2760.

[16] Chu TD, Chen CK. Modelling and model predictive control for a bicycle–rider system. Veh Syst Dyn. 2018;56(1):128–149.

[17] Wang P, Yi J, Liu T. Stability and control of a rider–bicycle system: analysis and experiments. IEEE Trans Autom Sci Eng. 2019;17:348–360.

[18] Schwab AL, De Lange PDL, Happee R, et al. Rider control identification in bicycling using lateral force perturbation tests. Proc Inst Mech Eng, Part K: J Multi-body Dyn. 2013;227(4):390–406.

[19] Dialynas G, Happee R, Schwab AL. Design and implementation of a steer-by-wire bicycle. Proceedings of the 7th Annual International Cycling Safety Conference; Available from: https://www.researchgate.net/publication/328808185.

[20] Francis BA, Wonham WM. The internal model principle of control theory. Automatica. 1976;12(5):457–465.

[21] Garcia CE, Morari M. Internal model control. a unifying review and some new results. Ind Eng Chem Process Des Dev. 1982;21(2):308–323.

[22] Wolpert DM, Ghahramani Z, Jordan MI. An internal model for sensorimotor integration. Science. 1995;269(5232):1880–1882.

[23] Gillespie RB, Ghasemi AH, Freudenberg J. Human motor control and the internal model principle. IFAC-PapersOnLine. 2016;49(19):114–119.
[24] Christoforidis C, Schouten AC, Happee R. Rider control identification in cycling taking into account steer torque feedback and sensorial delays [Master's Thesis]. under embargo, Delft University of Technology; 2019. Available from: http://resolver.tudelft.nl/uuid:2dbf0e15-a419-4267-ab6c-735409067d1a.
[25] Sanjurjo E, Naya MA, Cuadrado J, et al. Roll angle estimator based on angular rate measurements for bicycles. Veh Syst Dyn. 2019;57(11):1705–1719.
[26] Walpole SC, Prieto-Merino D, Edwards P. et al. The weight of nations: an estimation of adult human biomass. BMC Public Health. 2012;12:93. Available from: http://www.biomedcentral.com/1471-2458/12/439. DOI: 10.1186/1471-2458-12-439.
[27] Grasgruber P, Cacek J, Kalina T, et al. The role of nutrition and genetics as key determinants of the positive height trend. Econ Hum Biol. 2014;15:81–100. DOI: 10.1016/j.ehb.2014.07.002.
[28] Van Der Helm FC, Schouten AC, De Vlugt E, et al. Identification of intrinsic and reflexive components of human arm dynamics during postural control. J Neurosci Meth. 2002;119(1):1–14.
[29] De Vlugt E, Schouten AC, Van Der Helm FC. Adaptation of reflexive feedback during arm posture to different environments. Biol Cybern. 2002;87(1):10–26.
[30] Kawakami O, Kaneoke Y, Maruyama K, et al. Visual detection of motion speed in humans: spatiotemporal analysis by fmri and meg. Hum Brain Mapp. 2002;16(2):104–118.
[31] Barnett-Cowan M. Vestibular perception is slow: a review. Multisens Res. 2013;26(4):387–403.
[32] De Vlugt E, Schouten AC, Van Der Helm FC. Closed-loop multivariable system identification for the characterization of the dynamic arm compliance using continuous force disturbances: a model study. J Neurosci Meth. 2003;122(2):123–140.
[33] Happee R, De Vlugt E, Schouten AC. Posture maintenance of the human upper extremity; identification of intrinsic and reflex based contributions. SAE Int J Passenger Cars-Mech Syst. 2008;1(2008-01-1888):1125–1135.
[34] Miall R, Weir DJ, Wolpert DM, et al. Is the cerebellum a smith predictor? J Mot Behav. 1993;25(3):203–216.
[35] Smith O. Closed control of loops with dead time. Chem Eng Prog. 1957;53:217–219.
[36] Dialynas G, Christoforidis C, Happee R. The effect of haptic feedback in the balance task of bicycling. Symposium on the Dynamics and Control of Single Track Vehicles; Available from: https://www.researchgate.net/publication/337934996_The_effect_of_haptic_feedback_in_the_balance_task_of_bicycling.
[37] Mugge W, Abbink DA, Schouten AC, et al. A rigorous model of reflex function indicates that position and force feedback are flexibly tuned to position and force tasks. Exp Brain Res. 2010;200:325–340.
[38] Happee R, De Vlugt E, Van Vliet B. Nonlinear 2D arm dynamics in response to continuous and pulse-shaped force perturbations. Exp Brain Res. 2015;233(1):39–52.
[39] DJ Cole. A path-following driver–vehicle model with neuromuscular dynamics, including measured and simulated responses to a step in steering angle overlay. Veh Syst Dyn. 2012;50(4):573–596. Taylor & Francis.
[40] Newman MC. A multisensory observer model for human spatial orientation perception [PhD thesis]. Massachusetts Institute of Technology; 2009. Available from: https://core.ac.uk/download/pdf/4416187.pdf.
[41] Wada T. Computational model of motion sickness describing the effects of learning exogenous motion dynamics. Front Syst Neurosci. 2021;15:634604.
[42] Moore JK, Hubbard M, Kooijman JDG. A method for estimating physical properties of a combined bicycle and rider. ASME 2009 international design engineering technical conferences and computers and information in engineering conference. American Society of Mechanical Engineers; p. 2011–2020.

Appendices

Appendix 1 – Abbreviations

PID	proportional-integral-derivative feedback controller.
IMU	inertial measurement unit.
IRF	impulse response function.
FIR	finite impulse response.
CV	covariance coefficient.
VAF	variance accounted for.
DOP	discrete optimal predictor.
ZD	zero delay.
SD	sensory delay.
SDROP	sensory delay reafferent optimal predictor.

Mathematical notations

δ	steering angle.
ϕ	roll angle.
$\dot{\phi}$	roll rate.
θ	fork angle.
$\dot{\theta}$	fork rate.
$\dot{\delta}$	steer rate.
$T_{\text{PDH}}, T_{\text{PDF}}$	handlebar and fork applied torques of PD controller.
$K_{\text{PH}}, K_{\text{PF}}$	proportional handlebar and fork gains.
$K_{\text{DH}}, K_{\text{DF}}$	derivative gains of the handlebar and fork.
v	forward speed.
T_{ϕ}, T_{δ}	roll and steer rider torques.
$\theta_{\text{R}}, \theta_{\text{F}}$	rotation angle of the rear and front wheel.
$\dot{\theta}_R, \dot{\theta}_F$	rotational angular rates of the rear and front wheel.
y_P, y_Q	rear and front wheel contact points.
ψ	heading (yaw) angle.
l_g	force moment arm coefficient measured from the ground.
c_s	denotes the force relationship between roll and steer angle.
$y^{\delta}(t), y^{\phi}(t), y^{\psi}(t), y^{T\delta}(t)$	non-parametric output states of steer, roll, heading angle and steer torque
$\hat{y}^{\delta}, \hat{y}^{\psi}$	simulated disturbance output states.
$\grave{\text{E}}\c{s}^{\delta}{}_k, \grave{\text{E}}\c{s}^{\psi}{}_k, \grave{\text{E}}\c{s}^{T\delta}{}_k$	absolute magnitude limits of steer, heading angle and steer torque.
τ	time length of the impulse response function.
$h^{\delta}(\tau), h^{\phi}(\tau), h^{\psi}(\tau), h^{T\delta}(\tau)$	impulse response functions of steer, roll, heading angle and steer torque.
$w(t)$	external input force.
$K_{\dot{\phi}}, K_{\dot{\delta}}, K_{\phi}, K_{\delta}, K_{\psi}, K_{T_{\delta}}$	roll, steer, heading angle and steer torque gains.

Appendices II–V

Appendix II – Bicycle and neuromuscular dynamics models Appendix III – Predictor comparison, Appendix IV - Effects of rider body coupling analysed using a double pendulum model and Appendix V – Additional tables are available online here: https://doi.org/10.5281/zenodo.5818396 (Dialynas et al., 2019).